

Search for intrinsic NALs in BAL/mini-BAL quasar spectra

Daisuke Itoh,¹* Toru Misawa,² Takashi Horiuchi³ and Kentaro Aoki⁴

¹*Department of Physics, Faculty of Science, Shinshu University, 3-1-1 Asahi, Matsumoto, Nagano 390-8621, Japan*

²*School of General Education, Shinshu University, 3-1-1 Asahi, Matsumoto, Nagano 390-8621, Japan*

³*Ishigakijima Astronomical Observatory, National Astronomical Observatory of Japan, National Institutes of Natural Sciences, 1024-1 Arakawa, Isahaya, Nagasaki 854-0892, Japan*

⁴*Subaru Telescope, National Astronomical Observatory of Japan, 650 North Aohoku Place, Hilo, HI 96720, USA*

Accepted XXX. Received YYY; in original form ZZZ

ABSTRACT

Some fraction of narrow absorption lines are physically associated to the quasar/host-galaxy materials (i.e., intrinsic NALs) like those of BALs and mini-BALs. The relation between these three types of absorption lines has not been understood yet, however one interpretation is that these absorption features correspond to different inclination angles. In this study, we search for intrinsic NALs in 11 BAL/mini-BAL quasar spectra retrieved from VLT/UVES public archive, in order to test a possible relation of intrinsic NALs and BALs/mini-BALs in the geometry models. We use partial coverage analysis to separate intrinsic NALs from ones which are associated to cosmologically intervening materials like foreground galaxies and intergalactic medium (i.e., intervening NALs). We identify one reliable and two possible intrinsic NAL systems out of 36 NAL systems in 9 BAL/mini-BAL quasar spectra after removing two quasars without clear BAL features. In spite of a small sample size, we placed a lower limit on the fraction of BAL/mini-BAL quasars that have at least one intrinsic C IV NAL ($\sim 33^{+33}_{-18}\%$). This can be interpreted that intrinsic NAL absorbers exist everywhere regardless of inclination angle. We found that one of the intrinsic NAL systems detected in SDSS J121549.80-003432.1 is located at a large radial distance of $R > 130$ kpc, using a method of photoionization model with ground/excited-state lines. Considering the wide range of intrinsic NAL absorber distribution in inclination angles and radial distances, it suggests that origins and geometry of them are more complicated than we expected.

Key words: galaxies: active – quasars: absorption lines – quasars: general

1 INTRODUCTION

A substantial fraction of absorption lines in quasar spectra are physically associated to the background quasars (i.e., *intrinsic* absorption lines), rather than the other absorbers like intergalactic medium (IGM) or intervening galaxies (i.e., *intervening* absorption lines). They are caused by strong outflowing stream from accretion disk (i.e., outflow winds), and their offset velocities from the quasars are sometimes relativistic up to $\sim 0.3c$ (e.g., Hamann et al. 2018). There are several mechanisms for the accelerated outflow winds, including radiative pressure from the atomic lines and continuum (Murray et al. 1995; Proga et al. 2000; Proga & Kallman 2004; Proga et al. 2012), magneto centrifugal-force (Ev-

rett 2005), and thermal pressure (e.g., Chelouche & Netzer 2005). The outflow winds influence the evolutions of quasar host galaxies as well as the IGM surrounding them through (1) ejecting angular momentum from the quasar accretion disk to facilitate accretion onto the super-massive black hole (SMBH; Murray et al. 1995), (2) transporting metals and energy from the central engine to the host galaxies as well as the IGM and contributing to the chemical evolution of them (e.g., Dunn et al. 2010), (3) feeding back energy and momentum to inter-stellar medium (ISM) of the host galaxies to inhibit star formation (e.g., Di Matteo et al. 2005).

The intrinsic absorption lines in rest-frame UV spectra are usually classified into three categories: broad absorption lines (BALs) with $\text{FWHM} \geq 2,000 \text{ km s}^{-1}$, narrow absorption lines (NALs) with $\text{FWHM} \leq 500 \text{ km s}^{-1}$, and an intermediate subclass (mini-BALs). BALs and mini-BALs are

* E-mail: 18hs301e@shinshu-u.ac.jp (DI)

easily identified as intrinsic absorption lines because their large line width cannot be reproduced by thermal broadening or turbulence of intervening absorbers. On the other hand, it is not the case for NALs because a typical line width of intrinsic NALs are almost same as that of cosmologically intervening NALs, so it is difficult to classify them based on only visual inspection. There are several signs with which we can identify them as intrinsic NALs, including i) time variability of absorption profile and/or strength (e.g., [Hacker et al. 2013](#)), ii) partial coverage¹ (e.g., [Ganguly et al. 1999](#)) and iii) line-locking² (e.g., [Arav 1996](#)), and so on ([Hamann et al. 1997](#)). Based on partial coverage analysis, [Misawa et al. \(2007\)](#) found $\geq 50\%$ of optically bright quasars have at least one intrinsic NAL (see also [Simon, Hamann, & Pettini 2012](#)), which is larger than those for BALs ($\sim 10\text{--}20\%$; e.g., [Trump et al. 2006](#); [Gibson et al. 2009](#)) and mini-BALs ($\sim 5\text{--}10\%$; e.g., [Rodríguez-Hidalgo 2009](#)). These results suggests that roughly $\sim 70\%$ of quasars have at least one BAL, mini-BAL, and/or intrinsic NAL in their spectrum ([Hamann et al. 2012](#)). In particular, BAL is divided into three subclasses further based on a variation of detected absorption lines: HiBAL showing only relatively high-ionization lines (e.g., O v, N v, Si iv and C iv) as well as Ly α , LoBAL showing low-ionization lines (e.g., Al ii, Al iii, and Mg ii) in addition to the high-ionization lines above ([Voit, Weymann, & Korista 1993](#)), and an extreme class (FeLoBAL) showing very low-ionized iron lines as well (e.g., [Hazard et al. 1987](#); [Becker et al. 1997](#)).

There are two possible interpretations for detectability of BALs — (1) the orientation scenario, which suggests that quasars can be observed as BAL quasars only if our line of sight (LOS) to the continuum source of the wind quasars passes through the outflow wind (e.g., [Elvis 2000](#); [Ganguly et al. 2001](#)), and (2) the evolution scenario, which suggests that BAL quasars are in a particular (probably early) evolutionary stage and obscured by dust (e.g., [Borison & Meyers 1992](#); [Voit, Weymann, & Korista 1993](#); [Farrah 2007](#)), or they are in a state with high Eddington ratio and high black hole mass M_{BH} ([Giustini & Proga 2019](#)). While the evolution scenario has been suggested for LoBAL (especially for FeLoBAL) quasars ([Farrah 2007](#)), the orientation scenario is more likely for HiBAL quasars because BAL quasars and non-BAL quasars have similar emission line spectra except for BAL features (e.g., [Weymann et al. 1991](#); [Reichard et al. 2003](#)). Based on the orientation scenario, it is also suggested that quasars with narrower intrinsic absorption lines (i.e., mini-BALs and intrinsic NALs) are viewed at a smaller inclination angle relative to an axis of the accretion disk (unified model, hereafter; e.g., [Ganguly et al. 2001](#); [Hamann et al. 2012](#)) because in most cases, quasars with intrinsic NALs do not show any excess of X-ray absorption by warm absorbers that are located near the base of the outflow wind ([Misawa et al. 2008](#); [Chartas et al. 2009](#)). The numerical simulations of [Proga et al. \(2000\)](#) also show that the fast and dense streams which probably observed as BALs emerge at a larger inclination angle. Thus, the unified

model has often been used to understand the difference between BALs, mini-BALs, and intrinsic NALs. If the model is applicable for all quasars, neither mini-BAL nor intrinsic NAL is not expected to be detected in BAL quasar spectra. However, [Rodríguez-Hidalgo \(2009\)](#) detected mini-BALs in the BAL quasar spectra. Thus, an inclination angle toward which BAL or mini-BAL is detected has some overlap between them. For intrinsic NALs, it has not been systematically tested if they are present in a same inclination angle of BAL/mini-BAL quasar. [Ganguly et al. \(2001\)](#) reported there is an enhanced probability of detecting associated NALs in BAL quasar spectra, but those NALs are not classified into intrinsic and intervening ones.

In this study, we will confirm if *intrinsic* NALs are present in BAL/mini-BAL quasar spectra by separating intrinsic NALs from intervening ones with high-resolution spectra, to locate the origin of intrinsic NALs and test the unified model. This paper is structured as follows. In Section 2, we present sample selection and data reduction. A classification method of intrinsic NALs from intervening NALs is described in Section 3. The results and discussion are presented in Sections 4 and 5, respectively. In Section 6, we summarize our results. Throughout the paper, we use a cosmology with $H_0 = 75 \text{ km s}^{-1} \text{ Mpc}^{-1}$, $\Omega_{\text{m}} = 0.3$, and $\Omega_{\Lambda} = 0.7$.

2 SAMPLE SELECTION & DATA REDUCTION

For selecting sample quasars, we referred to the BAL quasar catalog in [Gibson et al. \(2009\)](#). This catalog contains 5039 BAL quasars that are identified based on modified Balnicity Index (BI₀) in any ions of C iv $\lambda\lambda 1548, 1551$, Si iv $\lambda\lambda 1394, 1403$, Al iii $\lambda\lambda 1855, 1863$ and Mg ii $\lambda\lambda 2796, 2803$, from the SDSS DR5 quasar catalog. BI₀ is essentially the same as traditional Balnicity Index (BI; [Weymann et al. 1991](#)), but integrate from 0 km s^{-1} instead of the traditional $3,000 \text{ km s}^{-1}$. Among the 5039 BAL quasars in [Gibson et al. \(2009\)](#), 25 BAL/mini-BAL quasars with Dec $< +15^\circ$ has been observed with VLT/UVES and already open to public in the archive, of which we use 11 BAL quasars as listed in Table 1 that satisfy all criteria below. First, quality of spectra should be high enough after combining all spectra taken within 7 days (spectral resolution of $R \geq 30,000$ and median signal-to-noise ratio of $S/N \geq 6$). Next, spectra should cover wavelength regions from Ly α emission lines to one of C iv, Si iv, and/or N v³ emission lines. If quasars have been observed in multiple epochs, we choose the one that have highest S/N ratio and largest wavelength coverage. All spectra in our sample are summarized in Table 2.

We retrieved raw data from the ESO archive⁴ and reduced them ourselves using the ESO Reflex workflow. The ESO archive provides both raw and reduced data so that we can carefully check a quality of spectra by comparing spectra reduced by the ESO archive and those by ourselves. After that, we applied a helio-centric velocity

¹ Absorbers do not cover the background flux source completely along our sight-line.

² The red member of a doublet is aligned with the blue member of the following doublet.

³ We do not use Mg ii doublet because [Jones et al. \(2010\)](#) show that low-ionized absorbers like Mg ii absorbers in molecular clouds could show partial coverage, even if they are intervening absorbers.

⁴ <http://archive.eso.org>

Table 1. Sample Quasars.

QSO name	RA (hh:mm:ss)	DEC (dd:mm:ss)	z_{em}	m_g (mag) ^a	m_r (mag) ^a	\mathcal{R}^b	L/Q ^c	BI ₀ (km s ⁻¹)
SDSS J022844.09+000217.0	02:28:44.1	+00:02:16.8	2.72	18.45	18.22	<3.08	Q	1962.9
SDSS J024221.87+004912.6	02:42:21.9	+00:49:12.0	2.06	18.50	18.20	<3.66	Q	896.2
SDSS J110855.47+120953.3	11:08:55.5	+12:09:53.3	3.67	20.14	18.60	<5.03	Q	213.0 ^d
SDSS J115122.14+020426.3	11:51:22.1	+02:04:26.4	2.40	19.06	18.60	<6.70	Q	156.0
SDSS J115944.82+011206.9	11:59:44.8	+01:12:07.2	2.00	17.58	17.24	450	L	937.9
SDSS J120550.19+020131.5	12:05:50.2	+02:01:30.0	2.13	17.46	17.08	<1.50	Q	403.9 ^d
SDSS J120917.93+113830.3	12:09:17.9	+11:38:27.6	3.11	17.64	17.47	<1.76	Q	323.5
SDSS J121549.80-003432.1	12:15:49.8	-00:34:30.0	2.71	17.50	17.35	<1.76	Q	4807.7
SDSS J122848.21-010414.5	12:28:48.2	-01:04:12.0	2.66	18.30	18.17	106	L	17.1
SDSS J133701.39-024630.3	13:37:01.4	-02:46:30.0	3.06	19.08	18.70	259	L	2.3
SDSS J143907.51-010616.7	14:39:07.5	-01:06:14.4	1.82	19.30	18.98	<8.2	Q	81.5

^a g or r -band magnitude referred from SDSS DR5.

^b Radio-loudness parameter, as defined in Section 2. We refer radio observation from FIRST survey. If radio source is undetected, we use the detection limit of the FIRST survey as an upper limit of the radio flux.

^c Classification of radio-loudness: radio-loud (L) or radio-quiet (Q), as defined in Section 2.

^d No clear BAL features are detected, although this is classified into BAL quasars in Gibson et al. (2009).

correction and an air-to-vacuum wavelength correction. If there are multiple spectra taken with same observing configuration within 7 days in the observed frame, we combine all of them as a single epoch to improve S/N ratio. We adopt 7 days as the maximum time interval for a single epoch because the shortest time scale of BAL variability in quasar rest-frame is a week to a month (Capellupo et al. 2011). Although C iv BALs sometimes exhibit significant equivalent width variability in a time scales of < 10 days, the fraction of epoch pair that exhibit significant BAL variability is very small ($\sim 3.7\%$, Hemler et al. 2019). Finally, we fitted the continuum and broad emission lines with a cubic spline function to make normalized spectra, except for heavily absorbed regions near emission lines (i.e., P-Cygni like regions). Based on our visual inspection, we found two quasars (SDSS J110855.47+120953.3 and SDSS J120550.19+020131.5) did not show clear BAL features, although these had been classified into BAL quasars. We will discuss these later in Section 4.

We also summarize radio-loudness of our sample quasars in Table 1. The Radio-loudness is defined as a ratio of the flux densities at 5 GHz and 4400 Å, i.e., $\mathcal{R} = f(5 \text{ GHz}) / f(4400 \text{ \AA})$. We derived $f(4400)$ from the SDSS g -band magnitude m_g assuming optical spectral index $\alpha_o = 0.44$ for all quasars, except for three (SDSS J110855.47+120953.3, SDSS J120917.93+113830.3 and SDSS J133701.39-024630.3 at $z_{\text{em}} > 3$), for which we used r -band magnitude m_r to avoid Ly α forest. As for the radio flux, we derived $f(5 \text{ GHz})$ from FIRST 1.4 GHz survey assuming a radio spectral index of $\alpha_r = 0.7$. According to the criterion of radio-loudness (i.e., $\mathcal{R} > 10$ as introduced by Kellermann et al. 1989), three out of the 11 BAL quasars are classified as radio-loud quasars. The fraction of radio-loud quasars among our sample is about 27%, which is consistent with the fraction among ordinary quasars ($\sim 10\text{-}20\%$; Kellermann et al. 1989; Urry & Padovani 1995; Ivezić et al. 2002) and also weakly consistent with that of BAL quasars (e.g., Tolea et al. 2002), although it seems to depend on both luminosity and redshift (Jiang et al. 2007; Bañados et al. 2015).

3 ANALYSIS

In this section, we first search for NALs in the 11 BAL quasar spectra (Sec. 3.1), and classify them into intrinsic and intervening NALs (Sec. 3.2 & 3.3) using partial coverage analysis.

3.1 Detection of NALs

We search for all of C iv $\lambda\lambda 1548, 1551$, Si iv $\lambda\lambda 1394, 1403$, and N v $\lambda\lambda 1239, 1243$ NALs that are detected with a confidence level of $> 3\sigma$; i.e., $[1 - R_{\text{abs}}]/\sigma(R_{\text{abs}}) > 3$, where R_{abs} and $\sigma(R_{\text{abs}})$ are residual flux and its uncertainty at the bottom of absorption line in the normalized spectrum. We also combine all NALs within 200 km s⁻¹ each other into a single absorption *system* as done in Misawa et al. (2007) because they are probably not physically independent. Finally, we prepare a homogeneous sample for statistical analyses below by removing NALs that are i) detected near P-Cygni profile (because continuum fitting is less reliable), ii) detected at low S/N region smaller than 6 pix⁻¹ (because line depth is less reliable), and/or iii) having equivalent width (EW) smaller than $4\sigma(\text{EW})$, where $\sigma(\text{EW})$ is 1σ uncertainty of equivalent width. We obtain 40 C iv and 12 Si iv NALs but no N v NAL in 45 NAL systems detected in the 11 BAL/mini-BAL quasar spectra, as listed in Table 3.

3.2 Partial coverage analysis

We use a partial coverage analysis to identify intrinsic NALs rather than time-variability or line-locking analysis because i) it requires only a single epoch spectrum while time variability analysis requires multiple epoch spectra and ii) NALs with partial coverage are frequently detected in $\sim 50\%$ of quasars while a line locking is very rare phenomena. Optical depth ratio of doublet lines by Lithium-like ions such as C iv, Si iv or N v should be 2:1 based on atomic physics. However, if absorbers do not cover the background flux source entirely along our LOS (i.e., partial coverage), the optical depth ratio would deviate from 2:1 (Hamann et al. 1997; Barlow & Sargent 1997). We can evaluate a fraction of flux

Table 2. Sample Quasar spectra taken from the ESO Archive.

QSO name	program ID	Wavelength range (Å)	Date	S/N [†]	Resolution
SDSS J022844.09+000217.0	081.A-0479(A)	4728-6838	2008/08/29	11.7	42310
SDSS J024221.87+004912.6	075.B-0190(A)	3283-4564	2005/09/05	7.1	40970
			2005/09/06	8.2	40970
				8.2	40970
		3732-5000	2005/09/05	13.1	40970
				13.5	40970
				12.2	40970
		5709-9464	2005/09/05	7.0	42310
	7.2		42310		
2005/09/06	6.4		42310		
SDSS J110855.47+120953.3	083.A-0042(A)	4583-6687	2009/04/16	7.6	34540
				6.7	34540
			2009/04/19	7.2	34540
				7.1	34540
			2009/04/20	7.4	34540
SDSS J115122.14+020426.3	092.B-0574(A)	3732-5000	2014/03/05	8.3	36840
				8.1	36840
		4583-6687	2014/03/06	7.6	36840
			2014/02/24	11.1	34549
			2014/02/26	11.2	34540
			2014/02/27	11.8	34540
SDSS J115944.82+011206.9	079.B-0469(A)	3703-5054	2007/06/06	15.1	40970
			2007/06/07	12.0	40970
		5603-9612	2007/06/06	9.3	42310
			2007/06/07	7.4	42310
SDSS J120550.19+020131.5	273.A-5020(A)	3282-4564	2004/05/17	13.1	40970
		4728-6837		14.2	42310
SDSS J120917.93+113830.3	080.A-0482(A)	4959-7071	2006/02/01	7.9	42310
SDSS J121549.80-003432.1	185.A-0745(D)	3282-4563	2011/03/28	6.4	49620
				7.6	49620
			2011/03/29	7.8	49620
		4583-6687		7.4	49620
			2011/03/28	13.3	51690
				15.1	51690
		4727-6835	2011/03/29	14.5	51690
				15.0	51690
			2011/03/30	7.6	51690
			12.0	51690	
			2011/03/31	13.8	51690
			11.0	51690	
			2011/04/01	11.4	51690
	12.3	51690			
SDSS J122848.21-01041.5	081.A-0334(A)	3259-4519	2008/04/07	6.2	40970
		4727-6835		12.1	42310
SDSS J133701.39-024630.3	091.A-0018(A)	4583-6687	2014/02/09	11.7	37820
			2014/02/10	11.9	37820
				11.8	37820
			2014/02/11	12.0	37820
SDSS J143907.51-010616.7	081.B-0285(A)	3732-5000	2008/05/01	5.6	40970
			2008/05/02	7.4	40970

[†] Median signal to noise ratio per exposure before combining other spectra.

that is covered by the absorber (i.e., Covering factor, C_f) by measuring residual flux of doublet lines by

$$C_f(v) = \frac{(1 - R_r(v))^2}{R_b(v) - 2R_r(v) + 1}, \quad (1)$$

where R_b and R_r are residual flux of blue and red members of doublet. If C_f is smaller than unity, the corresponding absorber is probably associated to the outflow winds, because the size of another possible candidate (i.e., foreground galaxies and intergalactic medium) is larger than the flux source by several orders of magnitude. We measure C_f by fitting absorption profile of NALs with Voigt profiles using the software package MINFIT (Churchill & Vogt 2001, hereafter, fitting method). The MINFIT is a line fitting code, with which we can perform a chi-square fitting using absorption redshift (z_{abs}), column density ($\log N$), Doppler parameter (b), and Covering factor (C_f) as free parameters. In the fitting process, we convolved a model profile with the instrumental line spread function. During the fitting trials, the code sometimes gives unphysical values of C_f such as $C_f > 1$ or $C_f < 0$, which tends to happen if absorption depth is very shallow and/or a real C_f value is close to unity. In such cases, we repeat a Voigt profile fitting assuming full coverage (i.e., $C_f = 1$) with no error bar for those components with unphysical C_f values in the first fitting trials as done in Misawa et al. (2007). In addition to the fitting method, we also measure C_f value for each *pixel* (hereafter, pixel-by-pixel method) to confirm the result of fitting method. Covering factor measured for each pixel is less reliable compared to that by the fitting method since the former is easily affected by photon noise as well as an instrumental line spread function in the wing parts of absorption trough (Ganguly et al. 1999). Therefore, we mainly use the results from the fitting method, while we use the pixel-by-pixel method in a supplementary way only if the fitting method does not give conclusive results.

3.3 Classification of NAL systems

We classified 52 NALs in 45 systems into three classes: class A (reliable intrinsic NALs), class B (possible intrinsic NALs), and class C (intervening or unclassified NALs) based on results of the fitting and the pixel-by-pixel methods, which is the same classification as introduced by Misawa et al. (2007). We classify all NALs into class A if they show a partial coverage with 3σ confidence level (i.e., $C_f + 3\sigma(C_f) < 1$) based on the fitting method. Among NALs that do not satisfy the criteria of class A, we search for class B NALs (i.e., possible intrinsic but less likely compared to class A) that satisfy the following criterion: they show partial coverage with 1σ confidence level (i.e., $C_f + \sigma(C_f) < 1$) based on the fitting method as well as the pixel-by-pixel method at the center. The other NALs are classified into class C that contains subclasses below: NALs consistent with full coverage (i.e., $C_f + \sigma(C_f) > 1$) for all components based on the fitting method as well as the pixel-by-pixel method (class C1), unclassified NALs because they are weak and blending with stronger components (class C2), and NALs for which we cannot apply reliable model fit because of continuum fitting and/or data defect such as blending with physically unrelated lines and noise spikes (class C3).

Among the five classes including subclasses, classes A, B, and C1 are those that are classified based on the partial

coverage analysis, while classes C2 and C3 are unclassified NALs because of severe line blending and/or low quality of the spectrum. We also apply the same classification for NAL *systems* as follows. If NAL systems contain at least one component that is classified into class A, we classify the system as a whole into class A regardless of the existence of class B and C NALs. In the same way, if NAL systems have at least one class B NAL but no class A NALs, we classify them into class B as a whole even if the other components are consistent with full coverage.

4 RESULTS

Using partial coverage analysis, we classify 45 NAL systems into 1 class A, 2 class B, and 42 class C systems, of which 29 are class C1, 3 are class C2, and 10 are class C3. Even if we remove two quasars without clear BAL features (as noted in Section 2), we still detect 1 class A and 2 class B NALs but smaller number (33) of class C NALs in 36 NAL systems. Thus, in BAL quasar spectra we detect three candidates for *intrinsic* NAL systems. All of them are identified with C iv NALs. In spite of rather small sample size, our result suggests that intrinsic NAL absorbers locate along our LOS to $\sim 33^{+33}_{-18}\%$ (3/9) of BAL quasars. Here, we would like to emphasize that the fraction is a lower limit because intrinsic NALs do not always exhibit partial coverage.

Table 3 summarizes parameters of 36 NAL systems in 9 BAL/mini-BAL quasars with clear BAL features as well as 9 NAL systems in two quasars without clear BAL features, including quasar name, emission redshift, ion name, wavelength in the observed frame, equivalent width in the observed frame, absorption redshift, offset velocity, column density, Doppler b parameter, covering fraction, NAL class, and other transitions of absorption lines detected in a same NAL system. Since emission redshift is sometimes blueshifted from the systemic redshift, offset velocities in the table could be underestimated by up to a few hundreds of km s^{-1} . On the other hand, our main fit parameter (i.e., covering factors) is not affected by the effect and still reliable.

Table 3. Properties of NALs, including quasar name in SDSS DR5 (QSO name), emission redshift (z_{em}), transition of absorption line (ION), observed-frame wavelength corresponding to a blue member of doublet (λ_{obs}), observed-frame equivalent width of a blue member of doublet (EW_{obs}), absorption redshift (z_{abs}), absorption redshift from background source (v_{off} : blueshift is positive), column density ($\log N$), Doppler b parameter (b), covering fraction C_f , NAL class (Class), and a list of other transitions of absorption lines that are detected at the same redshift (Other ions). Transitions in parenthesis are lines detected in the Ly α -forest (i.e., less reliable). For class C3 systems, we present only EW_{obs} , z_{abs} and v_{off} since we cannot place any meaningful constraints on fit parameters.

QSO name	z_{em}	ION	λ_{obs} (Å)	EW_{obs} (Å)	z_{abs}	v_{off} (km s $^{-1}$)	$\log N$ (cm $^{-2}$)	b (km s $^{-1}$)	C_f^\dagger	Class	Other ions
SDSS J022844.09+000217.0	2.72	C IV	5192.1	0.730	2.353	30994	13.75 ± 0.02	37.1 ± 2.2	1.00	C1	(Ly α , Si III λ 1207, Si II λ 1193)
					2.3536	30998	13.58 ± 0.18	11.7 ± 1.6	0.79 $^{+0.54}_{-0.31}$		
					2.3535	31008					
					2.446	22929					
					2.446	22912					
					2.4453	22973	15.38 ± 0.72	7.5 ± 1.4	0.98 $^{+0.16}_{-0.16}$		
					2.4459	22915	15.58 ± 0.61	9.3 ± 1.5	0.99 $^{+0.16}_{-0.16}$		
					2.4465	22864	14.16 ± 0.08	22.8 ± 3.0	0.91 $^{+0.16}_{-0.15}$		
					2.4468	22839	13.48 ± 0.04	5.3 ± 0.6	1.00		
					2.461	21646					
SDSS J022844.09+000217.0	2.72	C IV	5357.7	0.776	2.461	21646				C3	(Ly α)
					1.479	62454					
					1.4788	62458	13.29 ± 0.03	4.6 ± 0.5	1.00		
					1.4789	62450	13.47 ± 0.45	9.3 ± 6.0	0.52 $^{+0.50}_{-0.32}$		
					1.802	26592					
					1.8016	26598	13.73 ± 0.07	13.4 ± 1.1	0.96 $^{+0.08}_{-0.07}$		
					1.8017	26578	13.41 ± 0.02	9.0 ± 0.4	1.00		
					1.818	24849					
					1.8180	24857	13.32 ± 0.13	4.2 ± 0.5	0.92 $^{+0.15}_{-0.14}$		
					1.8181	24841	13.24 ± 0.02	6.5 ± 0.5	1.00		
SDSS J022844.09+000217.0	2.72	C IV	4337.4	0.510	1.802	26592				C1	(Ly α)
					1.818	24849					
					1.8180	24857	13.32 ± 0.13	4.2 ± 0.5	0.92 $^{+0.15}_{-0.14}$		
					1.8181	24841	13.24 ± 0.02	6.5 ± 0.5	1.00		
					1.933	12953					
					1.9320	13010	13.76 ± 0.01	9.2 ± 0.3	1.00		
					1.9327	12932	13.58 ± 0.11	14.3 ± 0.7	0.93 $^{+0.21}_{-0.16}$		
					1.9336	12843	12.96 ± 0.05	17.4 ± 2.7	1.00		
					1.946	11597					
					1.9450	11679	14.84 ± 0.22	33.2 ± 6.1	0.19 $^{+0.06}_{-0.06}$		
SDSS J022844.09+000217.0	2.72	C IV	4362.9	0.234	1.818	24849				C1	(Ly α)
					1.8180	24857	13.32 ± 0.13	4.2 ± 0.5	0.92 $^{+0.15}_{-0.14}$		
					1.8181	24841	13.24 ± 0.02	6.5 ± 0.5	1.00		
					1.933	12953					
					1.9320	13010	13.76 ± 0.01	9.2 ± 0.3	1.00		
					1.9327	12932	13.58 ± 0.11	14.3 ± 0.7	0.93 $^{+0.21}_{-0.16}$		
					1.9336	12843	12.96 ± 0.05	17.4 ± 2.7	1.00		
					1.946	11597					
					1.9450	11679	14.84 ± 0.22	33.2 ± 6.1	0.19 $^{+0.06}_{-0.06}$		
					1.9454	11647	17.26 ± 0.59	8.8 ± 1.0	0.18 $^{+0.06}_{-0.06}$		
SDSS J022844.09+000217.0	2.72	C IV	4540.1	0.750	1.933	12953				C1	(Ly α)
					1.9320	13010	13.76 ± 0.01	9.2 ± 0.3	1.00		
					1.9327	12932	13.58 ± 0.11	14.3 ± 0.7	0.93 $^{+0.21}_{-0.16}$		
					1.9336	12843	12.96 ± 0.05	17.4 ± 2.7	1.00		
					1.946	11597					
					1.9450	11679	14.84 ± 0.22	33.2 ± 6.1	0.19 $^{+0.06}_{-0.06}$		
					1.9454	11647	17.26 ± 0.59	8.8 ± 1.0	0.18 $^{+0.06}_{-0.06}$		
					1.9460	11579	14.53 ± 0.04	34.4 ± 2.3	0.56 $^{+0.06}_{-0.06}$		
					1.9468	11503	14.32 ± 0.21	24.3 ± 7.5	0.14 $^{+0.07}_{-0.06}$		
					1.946	11597					
SDSS J110855.47+120953.3	3.67	C IV	5783.7	2.996	2.736	12599	13.60 ± 0.01	6.1 ± 0.2	1.00	A	(N V λ 1239, 1243) Si IV λ 1393, 1403
					2.7346	65959	14.06 ± 0.05	32.5 ± 1.2	0.81 $^{+0.06}_{-0.06}$		
					2.7347	65950	13.72 ± 0.02	6.4 ± 0.2	1.00		
					2.7354	65903	13.69 ± 0.05	12.2 ± 0.7	0.98 $^{+0.06}_{-0.06}$		
					2.7357	65880	13.51 ± 0.08	8.1 ± 0.6	0.87 $^{+0.09}_{-0.09}$		
					2.7360	65852	13.72 ± 0.01	33.2 ± 0.6	1.00		
					2.7367	65803	14.28 ± 0.04	11.3 ± 0.5	0.97 $^{+0.05}_{-0.05}$		
					2.7369	65783					
					2.736	12599	13.60 ± 0.01	6.1 ± 0.2	1.00		
					2.7346	65959	14.06 ± 0.05	32.5 ± 1.2	0.81 $^{+0.06}_{-0.06}$		
SDSS J110855.47+120953.3	3.67	C IV	5783.7	2.996	2.736	12599	13.60 ± 0.01	6.1 ± 0.2	1.00	C1	(Ly α)
					2.7346	65959	14.06 ± 0.05	32.5 ± 1.2	0.81 $^{+0.06}_{-0.06}$		
					2.7347	65950	13.72 ± 0.02	6.4 ± 0.2	1.00		
					2.7354	65903	13.69 ± 0.05	12.2 ± 0.7	0.98 $^{+0.06}_{-0.06}$		
					2.7357	65880	13.51 ± 0.08	8.1 ± 0.6	0.87 $^{+0.09}_{-0.09}$		
					2.7360	65852	13.72 ± 0.01	33.2 ± 0.6	1.00		
					2.7367	65803	14.28 ± 0.04	11.3 ± 0.5	0.97 $^{+0.05}_{-0.05}$		
					2.7369	65783					
					2.736	12599	13.60 ± 0.01	6.1 ± 0.2	1.00		
					2.7346	65959	14.06 ± 0.05	32.5 ± 1.2	0.81 $^{+0.06}_{-0.06}$		

Table 3 – *continued* A table continued from the previous one.

QSO name	z_{em}	ION	λ_{obs} (Å)	EW_{obs} (Å)	z_{abs}	v_{off} (km s^{-1})	$\log N$	b (km s^{-1})	C_{f}^{\dagger}	Class	Other ions		
SDSS J115944.82+011206.9	2.00	C IV	4088.6	0.370	1.641	38014	13.94 ± 0.03	12.3 ± 0.3	$0.87^{+0.06}_{-0.06}$	B			
			3790.4	0.313	1.6409	38014							
			4211.2	1.475	1.720	29316					C3		
					1.720	29265						C1	
					1.7193	29352							
					1.7195	29321							
					1.7197	29304							
					1.7201	29262							
					1.7206	29206							
					1.7207	29197							
					1.7212	29135							
					1.7215	29113							
SDSS J120550.19+020131.5	2.13	C IV	4483.3	0.877	1.896	10566	12.68 ± 0.18	4.5 ± 2.1	1.00	C1			
					1.8954	10612							
					1.8956	10593							
					1.8956	10592							
					1.8959	10563							
					1.8962	10535							
					1.944	5667							
					1.9432	5707							
					1.9434	5682							
					1.9437	5653							
					1.9442	5607							
					1.944	5658							
SDSS J120550.19+020131.5	2.13	C IV	4102.6	0.640	1.944	5667	12.92 ± 0.29	13.6 ± 1.8	$0.88^{+1.00}_{-0.49}$	C2	Si II λ 1304, C II λ 1335, Si II λ 1527		
					1.9432	5707						Fe II λ 1606, Al II λ 1671, Fe II λ 2250	
					1.9434	5682							
					1.9437	5653							
					1.9442	5607							
					1.944	5658							
					1.591	56079							
					1.5902	56122							
					1.5905	56088							
					1.5908	56060							
					1.729	40927							
					1.747	38927							
SDSS J120550.19+020131.5	2.13	C IV	4224.3	0.395	1.729	40927	12.80 ± 0.08	8.4 ± 2.4	1.00	C1			
					1.747	38927							
					1.7467	38966							
					1.7470	38938							
					1.7471	38930							
					1.7472	38910							
					1.591	56079							
					1.5902	56122							
					1.5905	56088							
					1.5908	56060							
					1.729	40927							
					1.747	38927							
		1.7467	38966										
		1.7470	38938										
		1.7471	38930										
		1.7472	38910										
		1.591	56079										
		1.5902	56122										
		1.5905	56088										
		1.5908	56060										
		1.729	40927										
		1.747	38927										
		1.7467	38966										
		1.7470	38938										
		1.7471	38930										
		1.7472	38910										
		1.591	56079										
		1.5902	56122										
		1.5905	56088										
		1.5908	56060										
		1.729	40927										
		1.747	38927										
		1.7467	38966										
		1.7470	38938										
		1.7471	38930										
		1.7472	38910										
		1.591	56079										
		1.5902	56122										
		1.5905	56088										
		1.5908	56060										
		1.729	40927										
		1.747	38927										
		1.7467	38966										
		1.7470	38938										
		1.7471	38930										
		1.7472	38910										
		1.591	56079										
		1.5902	56122										
		1.5905	56088										
		1.5908	56060										
		1.729	40927										
		1.747	38927										
		1.7467	38966										
		1.7470	38938										
		1.7471	38930										
		1.7472	38910										
		1.591	56079										
		1.5902	56122										
		1.5905	56088										
		1.5908	56060										
		1.729	40927										
		1.747	38927										
		1.7467	38966										
		1.7470	38938										
		1.7471	38930										
		1.7472	38910										
		1.591	56079										
		1.5902	56122										
		1.5905	56088										
		1.5908	56060										
		1.729	40927										
		1.747	38927										
		1.7467	38966										
		1.7470	38938										
		1.7471	38930										
		1.7472	38910										
		1.591	56079										
		1.5902	56122										
		1.5905	56088										
		1.5908	56060										
		1.729	40927										
		1.747	38927										
		1.7467	38966										
		1.7470	38938										
		1.7471	38930										
		1.7472	38910										
		1.591	56079										
		1.5902	56122										
		1.5905	56088										
		1.5908	56060										
		1.729	40927										
		1.747	38927										
		1.7467	38966										
		1.7470	38938										
		1.7471	38930										
		1.7472	38910										
		1.591	56079										
		1.5902	56122										
		1.5905	56088										
		1.5908	56060										
		1.729	40927										
		1.747	38927										
		1.7467	38966										
		1.7470	38938										
		1.7471	38930										
		1.7472	38910										
		1.591	56079										
		1.5902	56122										
		1.5905	56088										
		1.5908	56060										
		1.729	40927										
		1.747	38927										
		1.7467	38966										
		1.7470	38938										
		1.7471	38930										
		1.7472	38910										
		1.591	56079										
		1.5902	56122										
		1.5905	56088										
		1.5908	56060										

Table 3 – *continued* A table continued from the previous one.

QSO name	z_{em}	ION	λ_{obs} (Å)	EW_{obs} (Å)	z_{abs}	v_{off} (km s ⁻¹)	$\log N$	b (km s ⁻¹)	C_f^\dagger	Class	Other ions
SDSS J120917.93+113830.3	3.11	C IV	5146.0	0.376	2.324	62746				C3	(Si II λ 1193, Ly α , C II λ 1335)
		C IV	5495.6	2.410	2.550	43658				C1	(Ly α)
							14.64 \pm 1.85	6.0 \pm 5.0	0.52 ^{+0.17} _{-0.15}		
							14.02 \pm 0.30	9.4 \pm 3.0	0.95 ^{+0.25} _{-0.25}		
							14.37 \pm 0.13	52.0 \pm 9.2	0.92 ^{+0.18} _{-0.16}		
							13.49 \pm 0.03	6.9 \pm 0.5	1.00		
							14.23 \pm 0.09	13.9 \pm 1.4	0.93 ^{+0.15} _{-0.15}		
							9127				
C IV	6172.4	1.241	2.987	9127					C3	(C III λ 977) Si IV λ 1393, 1403	
		Si IV	5605.8	1.685	3.022	6484				C3	(C III λ 977, C II λ 1036)
											Si II λ 1260, Si II λ 1304, C II λ 1335
SDSS J121549.80-003432.1	2.71	C IV	4637.5	0.495	1.995	63220	13.80 \pm 0.03	7.2 \pm 0.3	1.00 ^{+0.06} _{-0.06}	C1	(Si IV λ 1394, 1403)
							13.59 \pm 0.01	11.2 \pm 0.2	1.00		
							13.99 \pm 0.03	9.3 \pm 0.4	1.00 ^{+0.06} _{-0.06}	C1	(Si III λ 1207, Ly α Si IV λ 1394, 1403)
							13.56 \pm 0.01	37.1 \pm 1.2	1.00		
							13.31 \pm 0.14	5.3 \pm 0.7	0.93 ^{+0.18} _{-0.18}		
							13.11 \pm 0.29	6.2 \pm 1.0	0.66 ^{+1.00} _{-0.36}		
							13.26 \pm 0.11	11.2 \pm 0.6	0.64 ^{+0.11} _{-0.10}		
							12.92 \pm 0.01	5.0 \pm 0.2	1.00		
							12.87 \pm 0.01	14.3 \pm 0.5	1.00		
							13.10 \pm 0.11	13.7 \pm 1.2	0.82 ^{+0.28} _{-0.16}		
							13.28 \pm 0.05	4.5 \pm 0.2	0.98 ^{+0.06} _{-0.06}		
							13.29 \pm 0.04	9.9 \pm 0.4	0.94 ^{+0.06} _{-0.05}		
							12.39 \pm 0.03	4.0 \pm 0.5	1.00		
							12.76 \pm 0.56	5.6 \pm 2.7	0.27 ^{+1.00} _{-0.24}		
							12.53 \pm 0.45	4.4 \pm 0.8	0.59 ^{+1.00} _{-0.48}		
C IV	5355.0	2.736	2.459	20994					C1		
							13.59 \pm 0.17	18.1 \pm 3.6	0.71 ^{+0.60} _{-0.19}		
							13.61 \pm 0.01	9.1 \pm 0.2	1.00		
							13.47 \pm 0.02	4.7 \pm 0.2	1.00		
							14.09 \pm 0.04	38.3 \pm 1.7	0.98 ^{+0.05} _{-0.05}		
							13.94 \pm 0.05	6.0 \pm 0.4	1.00		
							14.16 \pm 0.03	11.0 \pm 0.7	1.00		
							13.52 \pm 0.02	6.3 \pm 0.3	1.00		
							13.65 \pm 0.22	22.6 \pm 5.7	0.78 ^{+0.78} _{-0.23}		

Table 3 – *continued* A table continued from the previous one.

QSO name	z_{em}	ION	λ_{obs} (Å)	EW_{obs} (Å)	z_{abs}	v_{off} (km s ⁻¹)	$\log N$	b (km s ⁻¹)	C_f^\dagger	Class	Other ions
SDSS J121549.80-003432.1	2.71	Si IV	4991.5	0.607	2.581	10583				C3	(Ly α) C IV $\lambda\lambda$ 1548,1551
		C IV	5685.4	0.464	2.672	3068	13.11 \pm 0.08	5.7 \pm 0.7	1.00	C1	(H I λ 1026, O VI $\lambda\lambda$ 1032,1038 Fe II λ 1062, Fe II λ 1125, Ly α)
					2.6716	3118	13.04 \pm 0.11	12.8 \pm 1.8	1.00		
					2.6718	3107	12.80 \pm 0.02	12.7 \pm 0.9	1.00		
					2.6730	3011	12.70 \pm 0.02	5.4 \pm 0.4	1.00		
					2.6734	2972					
		Si IV	5143.8	0.260	2.691	1570	13.40 \pm 0.05	2.9 \pm 0.3	1.00	C1	(C II λ 1036, O VI $\lambda\lambda$ 1032,1038 Si III λ 1193, Si III λ 1207)
					2.6902	1603	12.17 \pm 0.20	2.0 \pm 1.4	1.00		Ly α , Si II λ 1260, C II λ 1335
					2.6903	1596	12.94 \pm 0.75	15.2 \pm 5.3	0.31 ^{+1.00} _{-0.40}		
		C IV	5714.2	0.677	2.691	1549	14.24 \pm 0.03	6.0 \pm 0.1	0.95 ^{+0.03} _{-0.03}	B	
					2.6902	1602	13.37 \pm 1.25	21.3 \pm 5.0	0.11 ^{+0.06} _{-0.06}		
					2.6910	1537	13.40 \pm 0.09	12.5 \pm 0.4	0.68 ^{+0.26} _{-0.17}		
					2.6919	1466	13.08 \pm 0.23	4.5 \pm 0.5	0.38 ^{+0.37} _{-0.13}		
					2.6923	1435					
SDSS J122848.21-01041.5	2.66	C IV	4937.8	0.968	2.189	40651	13.45 \pm 0.44	11.4 \pm 2.7	0.48 ^{+1.00} _{-0.34}	C1	(Ly α , C II λ 1335)
					2.1881	40772	13.57 \pm 0.28	6.5 \pm 1.2	0.41 ^{+0.14} _{-0.12}		
					2.1886	40729	12.75 \pm 0.14	4.4 \pm 2.2	1.00		
					2.1894	40649	13.42 \pm 0.07	32.4 \pm 5.4	1.00		
					2.1897	40621					
					2.1899	40608	13.84 \pm 0.08	14.4 \pm 1.3	0.92 ^{+0.11} _{-0.10}		
		C IV	5143.1	1.237	2.322	28597	14.24 \pm 0.03	13.3 \pm 0.7	1.00	C1	(Ly α , H I λ 1026 Fe II λ 1134, Si III λ 1207)
					2.3218	28619	12.93 \pm 0.04	12.8 \pm 0.8	1.00		
					2.3220	28541	12.93 \pm 0.06	6.4 \pm 1.0	1.00		
					2.3226	28487	13.10 \pm 0.52	4.1 \pm 1.2	0.56 ^{+1.00} _{-0.43}		
					2.3229	28520					
		C IV	5561.8	0.352	2.592	5205	13.68 \pm 0.02	7.4 \pm 0.3	1.00	C1	(Ly α)
					2.5924	5203	13.14 \pm 0.29	4.6 \pm 0.7	0.80 ^{+1.00} _{-0.36}		N V $\lambda\lambda$ 1239,1243
					2.5945	5029					
		C IV	5636.0	0.190	2.640	1230	14.57 \pm 43.29	3.9 \pm 4.5	0.15 ^{+0.07} _{-0.07}	C2	(H I λ 972, O VI $\lambda\lambda$ 1032,1038 Ly α)
					2.6404	1225	13.16 \pm 0.12	65.3 \pm 22.8	1.00		
					2.6404	1224					

4.1 Intrinsic NALs in BAL quasars

We discovered intrinsic C iv NALs at $z_{\text{abs}} = 1.945$ in SDSS J024221.87+004912.6 (hereafter J0242+0049), at $z_{\text{abs}} = 1.641$ in SDSS J115944.82+011206.9 (hereafter J1159+0112) and at $z_{\text{abs}} = 2.961$ in SDSS J121549.80-003432.1 (hereafter J1215-0034). Among these, an identification of the NAL system in J0242+0049 is highly reliable because it shows a partial coverage with sufficiently high confidence level of $> 7\sigma$. We describe detailed properties of the three intrinsic NAL systems below.

4.1.1 Class A NAL at $z_{\text{abs}} = 1.945$ in J0242+0049

In the spectrum of J0242+0049 ($z_{\text{em}} = 2.062$, $m_g = 18.67$), there exist both a mini-BAL with an offset velocity from the quasar emission redshift (v_{off}) of $\sim 3,000 \text{ km s}^{-1}$ and a BAL with $v_{\text{off}} \sim 18,000 \text{ km s}^{-1}$. Hall et al. (2007) studied the mini-BAL and BAL systems in detail, and discovered that Si iv NALs corresponding to the C iv mini-BAL show line-locking between themselves. They also found the BAL is accelerated toward our LOS from June 2001 (SDSS data) to September 2005 (VLT/UVES data) by $0.154 \pm 0.025 \text{ cm s}^{-2}$.

This quasar has been observed only once with VLT/UVES in September 2005. The observed spectrum covers $\lambda \sim 3,300 - 5,000 \text{ \AA}$ and $\sim 5,700 - 9,400 \text{ \AA}$ with a typical spectral resolution of $R \sim 41,000$. The intrinsic C iv NAL at $z_{\text{em}} = 1.945$ is detected at wavelength region with sufficiently high S/N ratio of $\sim 17 \text{ pix}^{-1}$ for partial coverage analysis and is not overlapped with other absorption/emission lines. Best-fit model to the C iv NAL in Fig. 1 gives partial coverage of $C_f = 0.56 \pm 0.06$ for the main component, which satisfies the criterion of class A (i.e., $C_f + 7\sigma(C_f) < 1.0$).

As shown in Fig. 2, high-ionization lines such as N v⁵ with an ionization potential of IP = 98 eV and C iv (IP = 64 eV) are obviously detected, while low-ionization lines such as Al ii $\lambda 1671$ (IP = 19 eV), C ii $\lambda 1335$ (IP = 24 eV), and Mg ii $\lambda 2796, 2803$ (IP = 15 eV) are absent. An extremely high-ionized O vi $\lambda \lambda 1032, 1038$ line (IP = 138 eV) is not covered by the observed spectrum.

Since both N v and C iv NALs have smooth line profile with large line width (the flux-weighted line width of $\sigma_v \geq 100 \text{ km s}^{-1}$) that cannot be explained by thermal broadening only, their absorbers should have an external turbulence, which could be caused by a radiative pressure. Indeed, a large offset velocity of the NAL system from the quasar ($v_{\text{off}} \sim 11,600 \text{ km s}^{-1}$) supports that the corresponding absorber is an effectively accelerated outflow wind as frequently reported in the literature (Ganguly et al. 2007, Wild et al. 2008, Misawa et al. 2014).

4.1.2 Class B NAL at $z_{\text{abs}} = 1.641$ in J1159+0112

J1159+0112 ($z_{\text{em}} = 1.999$, $m_g = 17.59$), also known as Q1157+014 or PKS1157+014, is a radio-loud quasar (Wall et al. 1971). Ganguly et al. (2013) found that radio-loud quasars tend to have intrinsic absorption systems compared to radio-quiet ones, although the statistics for the former

⁵ We do not apply partial coverage analysis for the N v NAL because it is heavily blending with Ly α forest.

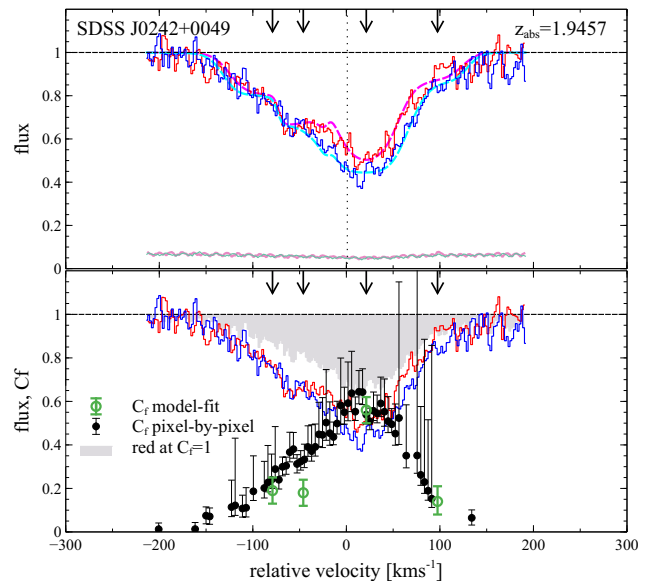


Figure 1. Best-fit model for C iv NAL at $z_{\text{abs}} = 1.945$ in BAL quasar J0242+0049. Downward arrows in both panels denote positions of absorption components. In the top panel, blue and red members of doublet are shown with blue and red histogram, while fitting results for them are shown with dashed cyan and magenta lines, respectively. Flux weighted line center is shown with a vertical dotted line. Bottom lines denote normalized 1σ errors. In the bottom panel, covering factors evaluated for each component or each pixel are plotted with green open circles or black filled circles. Shaded gray profile denotes a profile of C iv $\lambda 1551$ that is expected from the observed profile of C iv $\lambda 1548$ assuming a full coverage.

could be greatly affected by a single extraordinary object. Hayashi et al. (2013) placed a constraint on a viewing angle of the quasar smaller than $73 - 77^\circ$ with respect to the polar-jet based on radio polarimetric observations, while no constraint is placed on the lower limit. The quasar is not pole-on viewed at least, since it shows two-sided radio structures without significant polarization in its central component.

J1159+0112 has very strong C iv and N v BALs in the spectrum with FWHM of $> 3,000 \text{ km s}^{-1}$ around emission line peaks. In addition, there exists a mini-BAL system at $v_{\text{off}} \sim 8,000 \text{ km s}^{-1}$. Misawa et al. (2014) monitored the mini-BALs and detected an obvious time variability. The spectrum we use was taken with VLT/UVES in June 2007, covering a wavelength range of $\sim 3,700 - 5,000 \text{ \AA}$ and $\sim 5,600 - 9,600 \text{ \AA}$. The C iv NAL at $z_{\text{abs}} = 1.641$ is detected at wavelength region whose S/N ratio is large enough ($S/N \sim 18 \text{ pix}^{-1}$) for a partial coverage analysis. Best-fit model for the C iv NAL in Fig 3 provides a partial coverage of $C_f = 0.87 \pm 0.06$. Since both the fitting and the pixel-by-pixel methods support that a covering factor is smaller than unity with a confidence level of $> 2\sigma$, we classify the system into class B.

Our spectrum covers only wavelength regions corresponding to Si iv and Mg ii lines other than C iv, however, the former is severely blending with strong N v BAL and

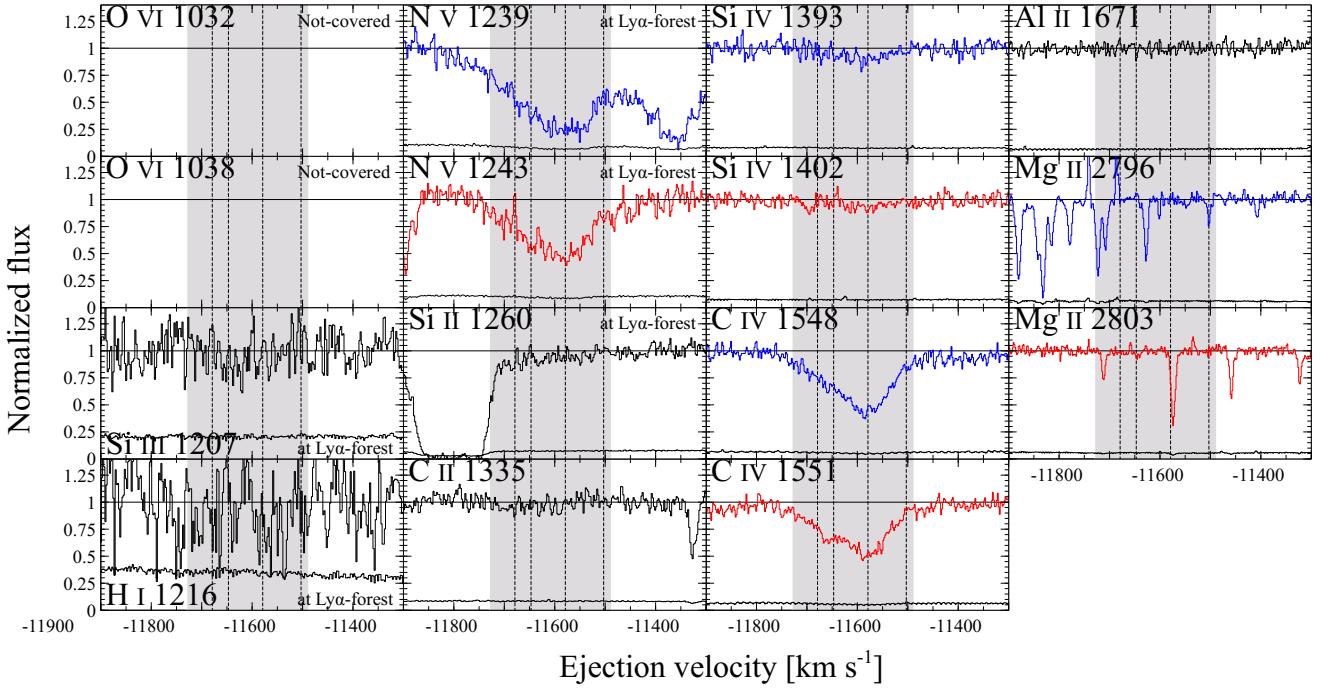


Figure 2. Velocity plot of NAL system at $z_{\text{abs}} = 1.945$ in J0242+0049. Zero velocity corresponds to the quasar’s emission redshift. Blue and red members of N v, Si iv, and C iv doublets are shown in blue and red histograms, respectively, while singlets are shown with black histograms. Shaded gray regions show the line width of the broadest absorption line without line blending in the system (i.e., C iv), where a normalized flux remains below 0.9. Vertical dashed-lines corresponds to the positions of components of the C iv NAL.

the latter is not clearly detected. Therefore, it is impossible to estimate the ionization condition of the NAL system.

This system has a quite large ejection velocity with $v_{\text{ej}} \sim 38,000 \text{ km s}^{-1}$, much larger than those of BAL and mini-BAL systems. Same as the case of J0242+0049, such a large offset velocity implies that this system is strongly accelerated by powerful quasar-driven outflow winds.

4.1.3 Class B NAL at $z_{\text{abs}} = 2.691$ in J1215-0034

The quasar J1215-0034 ($z_{\text{em}} = 2.71$, $m_g = 17.50$), also known as Q1213-003, has the strongest C iv (and also detected Si iv, N v and Ly α) BAL with $\text{BI}_0 = 4807.7 \text{ km s}^{-1}$ among our sample. This quasar was regarded as HiBAL quasar in [Bruni et al. \(2019\)](#). High resolution spectra ($R \sim 51690$) of the quasar were taken with VLT/UVES from March 28 to April 1 in 2011, covering a wavelength of $\sim 3,300 - 4,500 \text{ \AA}$ and $\sim 4,600 - 6,800 \text{ \AA}$.

A C iv NAL at $z_{\text{abs}} = 2.691$ is highly likely associated to the background quasar, the host galaxy, or its surrounding environments because its offset velocity from the quasar is smaller than $5,000 \text{ km s}^{-1}$ (i.e., an associated absorption line (AAL) as defined by [Weymann et al. 1997](#) and [Foltz 1986](#)). Since the C iv NAL is detected in the spectral region whose S/N ratio is quite high ($\sim 27 \text{ pix}^{-1}$), our result of the covering factor analysis is very reliable. The result of our fitting model to the C iv NAL is shown in Fig. 4, giving covering factor of $C_f = 0.95 \pm 0.03$ at the center. Since this result is consistent to the pixel-by-pixel method, we classify the NAL into class B. Our result is also visually inspected;

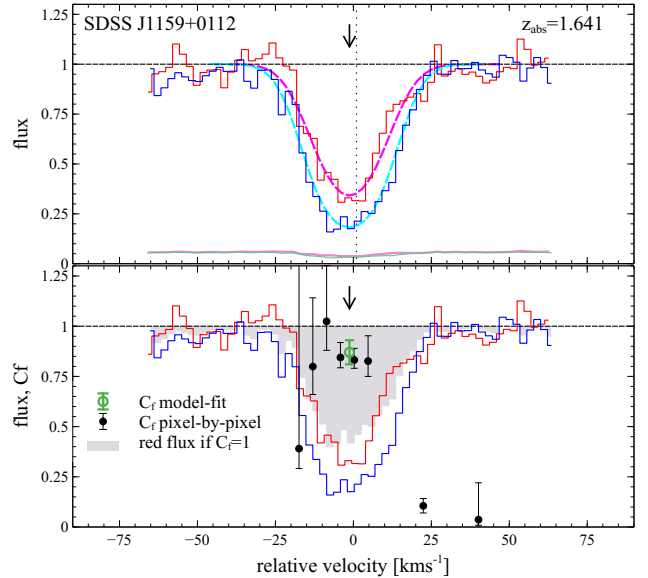


Figure 3. Same as Figure 1, but for C iv NAL at $z_{\text{abs}} = 1.641$ in J1159+0112.

both blue and red members of C iv doublet have almost the same absorption depth at the center with some residual flux (see Fig. 4), which is usually called as “non-black saturation”

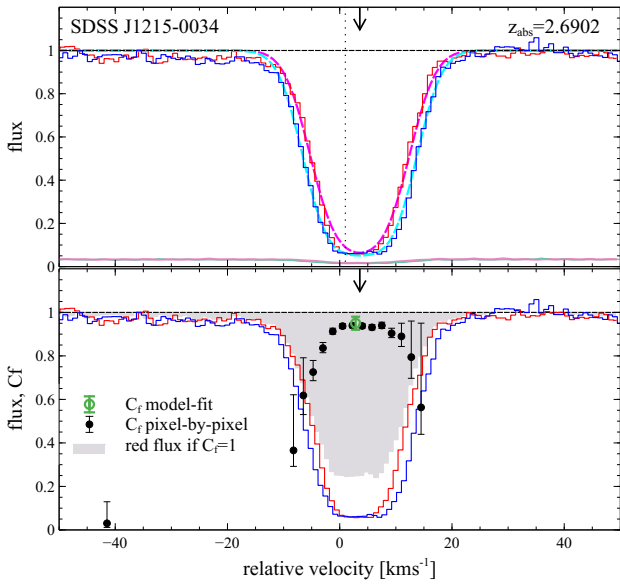


Figure 4. Same as Figure 1, but for C IV NAL at $z_{\text{abs}} = 2.691$ in J1215-0034.

and one of the most reliable signature of partial coverage. On the other hand, Si IV NALs in the same system are not showing partial coverage. However, this is not so surprising because partial coverage is often seen only in a part of transitions in same systems (Misawa et al. 2007). Since this system shows various ionic absorption lines from low-ions (e.g., C II and Si II) to high-ions (e.g., O VI) as shown in Fig. 5, it may have a complex ionization gradient inside it. Strong Ly α absorption line in this system has a large line width of FWHM $\sim 200 \text{ km s}^{-1}$ and almost saturated throughout the profile.

5 DISCUSSION

5.1 Intrinsic NAL Absorbers along Sight-lines toward BAL Quasars

Our detection of intrinsic (i.e., class A/B) NALs in BAL/mini-BAL quasar spectra suggests that intrinsic NAL absorbers locate along our LOS not only to non-BAL quasars but BAL/mini-BAL quasars. The detection rates of intrinsic NALs toward both types of quasars are roughly in agreement (i.e., $\sim 30\%$), but it should be regarded with some cautions because i) there is a large statistical uncertainty of our results for BAL/mini-BAL quasars with a detection rate of $33^{+33}_{-18}\%$ due to a small sample size, and ii) we placed only a lower limit on the detection rate since some fraction of intrinsic NALs could have a full coverage.

Misawa et al. (2007) found intrinsic C IV NALs in $\sim 32\%$ of non-BAL quasars at $z \sim 2-4$. Simon, Hamann, & Pettini (2012) also obtained a similar fraction for C IV NALs

($\sim 37\%$) in a velocity range of $v_{\text{off}} \sim 2,500 - 40,000 \text{ km s}^{-1}$. These results were obtained based on a partial coverage analysis as we adopted. Using time variability analysis, Wise et al. (2004) discovered that 4 out of 15 ($\sim 27\%$) quasars have at least one intrinsic C IV NAL at $v_{\text{off}} < 5,000 \text{ km s}^{-1}$. Nestor et al. (2008) had a slightly small value for the fraction ($\sim 14\%$) at $v_{\text{off}} < 12,000 \text{ km s}^{-1}$, but their result is based on a number excess of C IV NALs without identifying intrinsic NALs using low-resolution SDSS spectra. For further discussion to compare the detection rate of intrinsic NALs between BAL and non-BAL quasars, we need to increase (at least triple) our sample size that is comparable to the sample size of Misawa et al. (2007).

In the unified model of outflows, intrinsic NALs tend to be observed at small inclination angle relative to the rotational axis of the accretion disk, while BALs and mini-BALs are observed when our LOS passes through the outflow wind at larger inclination angle (i.e., closer to the accretion disk). In our analysis, however, we detect intrinsic NALs in spectra of $\sim 33^{+33}_{-18}\%$ of BAL quasars, which suggests that the location of intrinsic NAL absorbers are not limited to the regions at higher latitude but they exist everywhere regardless of inclination angle. Thus, the simple unified model of outflow wind is not applicable.

5.2 Radial Distance of NAL system at $z_{\text{abs}} = 2.691$ in J1215-0034

As shown in Fig. 5, we detected Si II and C II lines in the NAL system at $z_{\text{abs}} = 2.691$ in J1215-0034. Since Si⁺ and C⁺ ions have three electrons at outermost electron shell, the ground electron state has two fine-structure levels (true ground $J = 1/2$ and slightly excited $J = 3/2$). As done in the literature (e.g., Barlow & Sargent 1997; Hamann et al. 2001; Borguet et al. 2012; Chen et al. 2018), it is possible to estimate a gas density and a radial distance of absorbers from the central source using photoionization model for absorption systems with both ground and excited levels such as S IV^{*}/S IV, Si II^{*}/Si II, C II^{*}/C II and Fe II^{*}/Fe II. An ionization parameter U , the ratio of hydrogen-ionizing photons illuminated to absorber (n_{γ}) and the total hydrogen number density (n_{H}) is defined as

$$U \equiv \frac{n_{\gamma}}{n_{\text{H}}} = \frac{Q(\text{H})}{4\pi c n_{\text{H}} R^2}, \quad (2)$$

where $Q(\text{H})$ is the hydrogen-ionizing photon number rate emitted by central source, and R is a distance of absorbers from the central source.

To measure a radial distance R , we also need to know n_{H} . In highly ionized zone, the relation between the n_{H} and an electron density n_{e} is approximately shown as $n_{\text{e}} \sim 1.2n_{\text{H}}$. The n_{e} can be estimated using a column density ratio of ground and excited levels by

$$n_{\text{e}} = n_{\text{cr}} \left[\frac{N_{\text{l}}}{N_{\text{u}}} \left(\frac{g_{\text{u}}}{g_{\text{l}}} \right) e^{-\Delta E/kT} - 1 \right]^{-1}, \quad (3)$$

where N_{l} and N_{u} are column densities of ground and excited levels, $g_{\text{u}} / g_{\text{l}}$ is a ratio of statistical weight, ΔE is the energy difference between the two-levels (e.g., 63.42 cm^{-1} for C II^{*} and C II from the NIST Atomic Spectra Database

⁶ The fraction would be $\sim 50\%$ if we also consider N V and Si IV in addition to C IV.

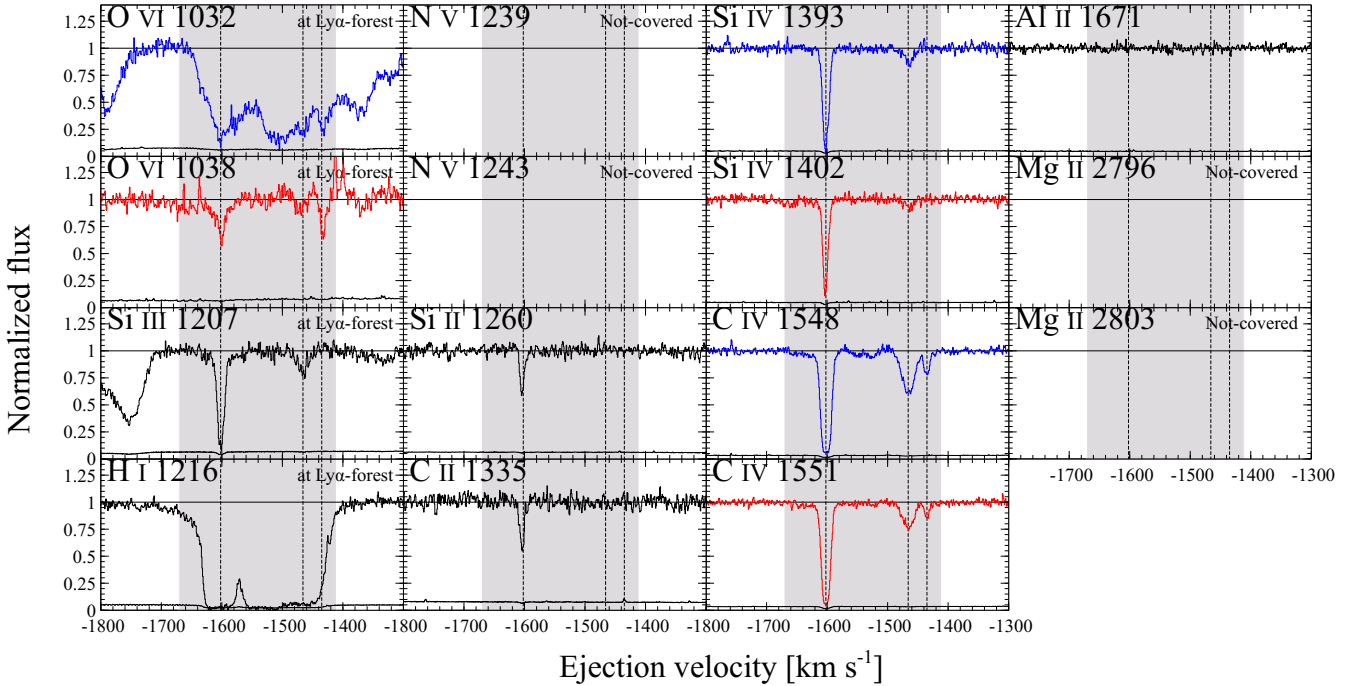


Figure 5. Same as Figure 2, but for NAL system at $z_{\text{abs}} = 2.691$ in J1215-0034. Shaded gray regions show the line width of the broadest absorption line without line blending in the system (i.e., Ly α), where a normalized flux remains below 0.9.

⁷), k is Boltzmann constant, T is a nominal temperature of ionized plasma, and n_{cr} is the critical density for excited and ground state ($\sim 50 \text{ cm}^{-3}$ at $T \sim 10^4 \text{ K}$ for C II*/C II; e.g., Goldsmith et al. 2012).

We assume an ionization parameter of $\log U \sim -2.0$ based on the ratio of column density of C II/C IV and Si II/Si IV from CLOUDY models in Hamann (1997). We also need SED models for estimating an ionizing photon rate $Q(\text{H})$. The MF87 SED (Mathews & Ferland 1987) has been widely used as a typical AGN SED model. However, as discussed in Dunn et al. (2010) and Arav et al. (2013), the MF87 model could be only applicable for radio-loud quasars. For radio-quiet quasars, it is recommended to use UV-soft SED model (i.e., not showing UV-bump around 600 \AA). Because J1215-0034 is a radio-quiet quasar with a radio-loudness of $\mathcal{R} < 1.76$ (see Table 1), we use a UV-soft SED below. From near-UV (NUV) to far-UV (FUV) region (i.e., $912 - 3,000 \text{ \AA}$), we adopt spectral index $\alpha_{\text{UV}} = -0.61$ from Lusso et al. (2015) and scale it to UV flux of J1215-0034. Lusso et al. (2015) have determined an average spectral index from NUV, FUV, to extreme-UV (EUV), for high-redshift ($2.3 < z_{\text{em}} < 2.6$) and bright ($g < 18.5 \text{ mag}$) quasars. The quasar J1215-0034 ($z_{\text{em}} = 2.71$ and $g = 17.50 \text{ mag}$) roughly satisfy the criteria above. In X-ray, we adopt spectral index $\alpha_{\text{X}} = -0.61$ and optical-to-X-ray slope $\alpha_{\text{OX}} = -1.62$ from observations with Chandra (Martocchia et al. 2017). Finally, we interpolate a power law between FUV and X-ray to estimate an SED in EUV which is observationally un-

available. We show the estimated SED model in Fig. 6. As a result, we calculate $Q(\text{H}) = 2.43 \times 10^{57} \text{ s}^{-1}$.

We detect ground levels of Si II and C II lines in the NAL system, but no remarkable profiles are detected for excited levels. Therefore, it is possible to place an upper limit on n_e and a lower limit on R , using equations 2 and 3. Because n_{cr} of C II is smaller than that of Si II, we calculate these limits only for C II line to place more stringent constraints on n_e and R . While we estimate a column density of ground level of C II line as $\log N_l(\text{cm}^{-2}) = 13.05$, we place only upper limit on it for C II* as $\log N_u(\text{cm}^{-2}) \leq 12.23$ assuming 1σ uncertainty of continuum level. Fig. 7 shows modeled profiles of ground levels of C II line. The ratio of column density between ground and excited levels is $N_u / N_l \leq 0.15$, which leads to an upper limit on the electron density ($n_e \leq 4.1 \text{ cm}^{-3}$), and a lower limit on the distance of absorber is $R \geq 141 \text{ kpc}$, as shown in Fig. 8.

Possible concern about this calculation is how much an incident ionizing flux from the continuum source is dimmed by BAL absorber. Because the NAL system locates along our LOS to the quasar behind the BAL absorber, we could overestimate ionizing photons to the NAL absorber. If we simply assume that ionizing photons are partially absorbed only by neutral hydrogen in the BAL absorber, an optical depth at the Lyman limit is

$$\tau_{\text{LL}} = N_{\text{HI}} \sigma_{\text{H}}^0 \quad (4)$$

where $\sigma_{\text{H}}^0 = 6.3 \times 10^{-18} \text{ cm}^2$ is the H I cross section at the Lyman limit and N_{HI} is H I column density of the BAL system. We evaluate N_{HI} applying apparent optical depth method (i.e., AOD, Savage & Sembach 1991) to the Ly α BAL. Using equations (10) and (11) from Savage & Sembach

⁷ <https://physics.nist.gov/asd>

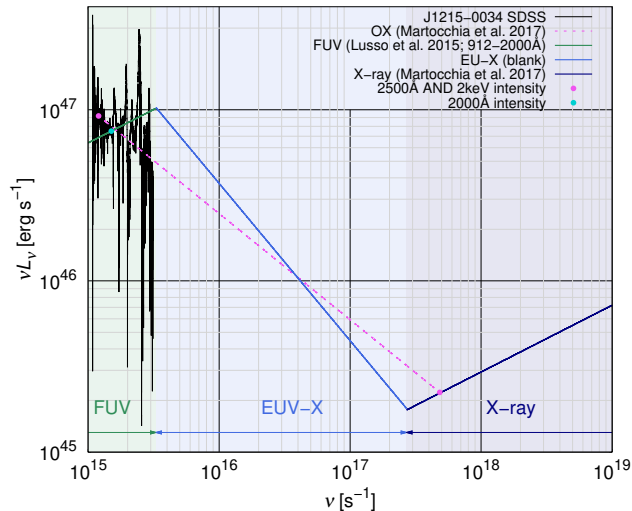


Figure 6. The SED model of J1215-0034. We plotted SDSS spectrum of J1215-0034 in black solid line. We used at 2000 Å intensity (cyan circle) for normalizing SED models. Magenta circle and dot line represent 2500 Å and 2keV monochromatic luminosity ratio (using result of Martocchia et al. 2017). The solid lines of green, blue and dark-blue represent SED models of FUV, EUV-X and X-ray regions, respectively.

(1991), we estimate $\log N_{\text{H}}(\text{cm}^{-2}) = 16.10$, and a fraction of ionizing photons that are attenuated by the BAL absorber is only $\sim 10\%$. Even if we consider this correction, a lower limit of the radial distance is still large ($R \geq 133$ kpc). Therefore, we conclude that the NAL system locates at a large distance comparable to a scale of Circum-galactic medium (CGM)⁸ which is several orders of magnitude larger than the typical scale of radiation-driven wind at $\sim 0.01 - 0.1$ pc (Murray et al. 1995, Proga et al. 2000).

5.3 Two types of intrinsic NALs

5.3.1 Intrinsic NAL in J1215-0034

This NAL system is a typical associate absorption line (AAL) because it has a small ejection velocity ($v_{\text{off}} \sim 1,600 \text{ km s}^{-1}$). Possible origins of AAL absorbers include i) AGN outflow winds in pc to sub-pc scale, ii) materials associated with quasar host galaxies, and iii) cluster/group of galaxies around of the quasar. Among these, Wild et al. (2008) concluded that about 40% of C IV AALs with $v_{\text{off}} \leq 3,000 \text{ km s}^{-1}$ are probably physically associated with the quasars themselves and its host galaxies [i.e., case i) and ii) above]. If we assume C IV broad emission line region (BELR) is a background source, the size of NAL absorber is smaller than the size of BERL $R_{\text{CIV}} = 0.12 \pm 0.10$ pc, where we use an equation (1) in Lira et al. (2018). This size is much smaller than the size of typical cosmologically intervening

⁸ This is not a scale of the IGM since the size of CGM is usually defined as a virial radius r_{vir} , which is ~ 200 kpc for L^* galaxies (Tumlinson et al. 2017).

absorbers (i.e., 1 – 100 kpc). Thus, among the three possible origins the case iii) is less likely since the corresponding size of absorbers (\sim kpc) is much larger than the size of BELR.

Among the other possible origins, the case i) is also rejected because the absorber’s radial distance from the central source ($R > 130$ kpc) is much larger than the typical radial distance of radiation-driven outflow wind (i.e., 0.01 – 0.1 pc). Thus, our results suggest the NAL system most likely originates in materials associated with quasar host galaxies or CGM around it.

Indeed, recent results of radial distance measurements of BAL/mini-BAL absorbers with photoionization models using ground/excited state lines implies that they sometimes spread up to 0.1 – 10 kpc (Moe et al. 2009; Dunn et al. 2010; Aoki et al. 2011; Borguet et al. 2013; Chamberlain et al. 2015; Arav et al. 2018; Xu et al. 2018) or > 10 kpc (Hamann et al. 2001; Hutsemekers et al. 2004; Borguet et al. 2012) from the central source. Faucher-Giguère et al. (2012) proposed a model that BAL absorbers especially for LoBAL ones form in situ in the ISM of the host galaxy. For intrinsic NALs, Wu et al. (2010) estimated their radial distance as 0.01–10 kpc from the central source based on photoionization models. Considering these results, intrinsic NAL absorbers at a large distance with $R > 100$ kpc may have some relationship with such kilo-parsec scale BAL/NAL absorbers. They could be decelerated while interacting with materials in/around host galaxies, and eventually contributing to energy/momentum feedback to host galaxies, CGM, and IGM around them.

The NAL system has other possible origins since there exist a point source ~ 5 arcsec (corresponding to ~ 40 kpc at $z \sim 2.69$) north-west of J1215-0034 both in *Chandra* X-ray and SDSS DR16 optical images. If this is a foreground faint AGN at $z \sim 2.69$, the NAL system could be due to outflow wind from the AGN whose opening angle is large enough to cover our LOS to J1215-0034. Alternatively, if this point source is a normal galaxy (i.e., inactive galaxy), its CGM could produce the NAL at $z \sim 2.69$. If the latter is the case, the corresponding absorber should be in a special condition because its size is small enough not to cover the background flux source of J1215-0034 despite being an intervening absorber.

Recently, Balashev et al. (2020) discovered a proximate Damped Ly α system (PDLA) with a partial coverage at a distance of $\sim 150 - 200$ kpc from the background quasar. They infer the PDLA originates from a galaxy located in a group where the quasar-host galaxy resides. The properties (i.e., size and radial distance) of this PDLA is very similar to those of the class B NAL in J1215-0034. If this NAL system originates in an absorber like a PDLA above, some fraction of intrinsic NAL systems in the past studies could also have similar origins (i.e., absorbers in member galaxies in group/cluster around quasar host galaxies). In the current study, we conclude that the NAL system at $z \sim 2.69$ is physically associated to J1215-0034 (i.e., intrinsic NAL) based on our already available data, however, we will conduct spectroscopy of the point source ($m_g \sim 21.3$) to locate its origin as a future work.

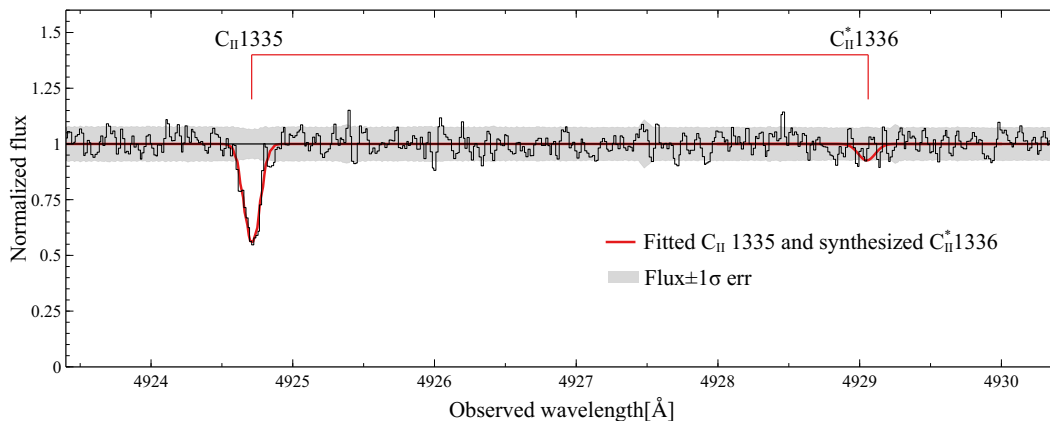


Figure 7. Observed (black histogram) and modeled (red curves) profiles of ground C II 1335 and excited C II* 1336 lines in a spectrum of J1215-0034. The shaded gray region show 1σ uncertainty of continuum flux.

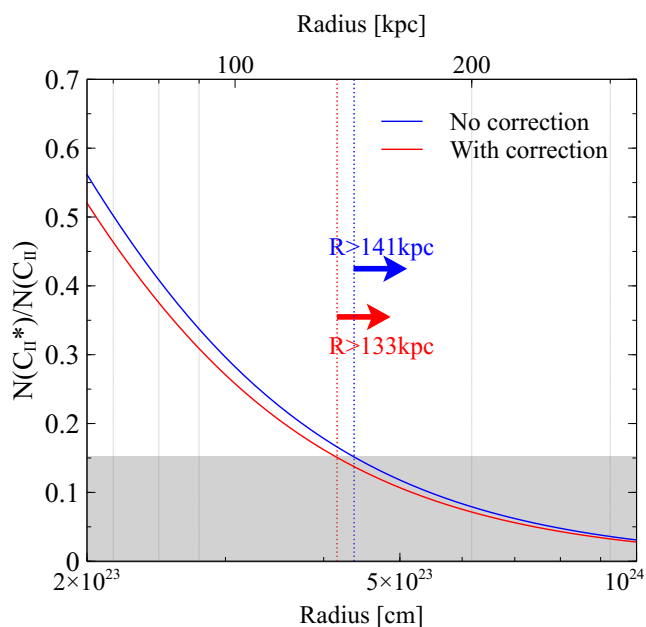


Figure 8. Line ratio of C II* and C II as a function of radial distance for the intrinsic NAL absorber in J1215-0034. The blue and red curves show the relations without and with BAL absorption correction. The shaded region in gray indicates $N(\text{C II}^*)/N(\text{C II}) < 0.15$, corresponding to a radial distance of $R > 141$ kpc (blue dotted line) and $R > 133$ kpc after the correction of the BAL attenuation (red dotted line), respectively.

5.3.2 Intrinsic NALs in SDSS J024221.87+004912.6 and J1159+0112

For the other two intrinsic NAL systems, we cannot place strong constraints on their radial distance without detecting either time variability or absorption lines from fine-structure levels. However, we have several important properties of them.

The NAL system in J0242+0049 shows three signs of intrinsic origin: a) only high-ionization absorption lines such as N V, C IV (and possible Si IV) are detected without any remarkable detection of low-ionization lines as shown in Fig 2,

b) it has very large ejection velocity of $\sim 11,600 \text{ km s}^{-1}$ with relatively broad ($\sigma_v > 100 \text{ km s}^{-1}$) and smooth line profile, and c) it shows a reliable (i.e., class A) partial coverage along LOS to the continuum source with size of $\sim 0.01 \text{ pc}$. These properties strongly support that the NAL system indeed originates in a small clumpy (or filamentary) structure in central region of the outflow wind, and being accelerated by radiation-pressure. Such a small scale clumpy structure is frequently reproduced by two/three-dimensional radiation-magnetohydrodynamic simulations caused by hydrodynamic instability in the innermost region of outflow wind (Ohsuga et al. 2005, Takeuchi et al. 2013, and Kobayashi et al. 2018). Although only C IV line is detected in another NAL system in J1159+0112, it also has some properties of intrinsic NALs like partial coverage and large ejection velocity ($\sim 38,000 \text{ km s}^{-1}$). It could be in a same environment as the NAL system above but being accelerated more efficiently.

5.4 NAL/BAL absorbers at large and small radial distances

In the previous section, we discuss two extreme types of intrinsic NAL absorbers: a high-ionized NAL with large ejection velocity in J0242+0049 and a low-ionized NAL with small ejection velocity in J1215-0034 (we cannot classify the NAL in J1159+0112 because only C IV is detected). The former is probably related to the outflow wind that is being radiatively accelerated at a small distance from the continuum source, while the latter locates at a large distance comparable to the scale of CGMs. Thus, these NAL systems may correspond to different types of absorbers.

Indeed, such a large difference in a radial distance has been suggested for BAL absorbers repeatedly. As a traditional method, a variability time scale of BAL strength/profile has been used for calculating a radial distance of BAL absorbers assuming a Keplerian motion. This method tends to give small distances (e.g., $R < 10 \text{ pc}$; Capellupo et al. 2011; Rodriguez-Hidalgo et al. 2011; Muza-hid et al. 2016; Moravec et al. 2017; McGraw et al. 2017).

Another method of calculating absorber's distance based on photoionization models would lead to larger values. For example, a distance of $\sim 1 - 10 \text{ kpc}$ was evaluated

by comparing line strengths of ground/excited levels of relatively low-ionized ions (Si II, C II and Fe II) with a small ejection velocity $\sim 5,000 \text{ km s}^{-1}$ (Moe et al. 2009; Dunn et al. 2010; Aoki et al. 2011). If higher ionized ions like S IV with larger ejection velocity of $\sim 10,000 \text{ km s}^{-1}$ are used, the value would be somewhat smaller, $\sim 0.1 \text{ kpc}$ (Borguet et al. 2013; Chamberlain et al. 2015; Arav et al. 2018; Xu et al. 2018).

Here, we would like to emphasize a measured radial distance depends on calculating methods. For example, we tend to derived a small radial distance based on time variability analysis assuming a gas motion since outflow winds which locate in the vicinity of central source are rotating much faster than those at large radial distance ($> 1 \text{ kpc}$). This trend is consistent to the past results that BALs with large ejection velocity (i.e., rapidly rotating around the central source) tend to show time variability in smaller time scales compared to those with smaller ejection velocity (Capellupo et al. 2011).

5.5 Possible geometry of BAL and intrinsic NAL absorbers

We conclude that an inclination angle alone cannot be a good indicator to distinguish intrinsic NAL from BAL absorbers as frequently introduced in the literature, because 1) intrinsic NALs are detected regardless of an existence of BAL/mini-BAL features in quasar spectra, and 2) both BAL and intrinsic NAL absorbers distribute over a wide range of radial distance from the central source (§ 5.4).

We present a possible structure of outflow winds based on our results in Fig. 9, in which there exist both small distance absorbers at pc-scale and large distance ones at kpc-scale or more. The size of intrinsic NAL absorbers should be smaller than the central flux source because of partial coverage. The small distance absorbers are probably related to the radiation-driven outflows near the center and accelerated up to $\sim 0.1c$, depending on the acceleration efficiency and/or an inclination angle. On the other hands, the large distance outflows are probably extended outflow winds (e.g., Chen et al. 2018) that are formed (and decelerated) by interaction with ISM and CGM of host galaxies. In this model, we are able to observe intrinsic NALs in any inclination angles.

It could be possible that some fraction of BALs and intrinsic NALs have same origins but their line width depends on a number of small scale clumpy clouds (i.e., larger number of clouds would produce broader absorption profile like BALs). Lu & Lin (2018a,b, 2019) attempted to classify BALs into two subclasses: Type S BALs (BALs with smooth trough) and Type N BALs (BALs with multiple components like NALs), and suggested that the latter is essentially originated in same absorbers as intrinsic NALs. Our results supports the scenario.

6 CONCLUSION

In this study, we search for intrinsic NALs in 11 BAL/mini-BAL quasar spectra using partial coverage analysis, to test whether intrinsic NALs are detected along with BALs/mini-BALs. We summarized our results below:

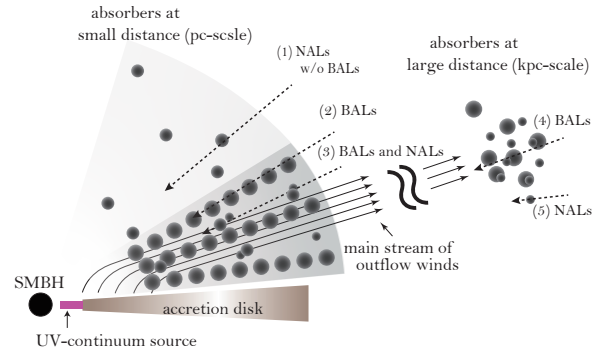


Figure 9. Possible geometry of outflowing absorbers. At smaller distances, there exist small clumpy clouds (black sphere) that can be observed as intrinsic NALs. The main stream of outflow wind consisting of a large number of clumpy clouds would be observed as BALs. At larger distances, clumpy clouds are formed by interaction between outflow gas and ISM/CGM of host galaxy and they are observed as BALs/NALs depending on how many clouds are clustering. Dashed line (1) represents a LOS along which we observe intrinsic NALs at small inclination angles. Dashed lines (2) and (3) are LOS for BALs, but only in line (3), clumpy clouds with different offset velocity from BAL absorber are observed as intrinsic NALs in addition. At large distances, absorption line width also depends on a number of clumpy clouds as shown with two dash lines (4) and (5).

(i) We identified one reliable (class A) and two possible (class B) intrinsic NAL system in 3 of 9 quasars with clear BAL profiles, which suggests that the location of intrinsic NAL absorbers are not limited to the regions at higher latitude and that they exist everywhere regardless of inclination angle.

(ii) Using photoionization model with ground/excited levels of C II absorption line, we estimated a radial distance of intrinsic NAL absorber in J1215-0034 as $R > 140 \text{ kpc}$ that is comparable to the scale of the CGM of host galaxy. A lower limit of radial distance is still large ($R > 130 \text{ kpc}$) even after considering flux dimming by the BAL absorber along the same LOS.

(iii) The intrinsic NAL system in J0242+0049 showing possible partial coverage may originate in small clumpy clouds at small radial distance because it has a large ejection velocity and high ionization condition, while the NAL system in J1215-0034 has opposite properties (i.e., small ejection velocity and low ionization condition).

(iv) Intrinsic NAL systems in J1215-0034 and J0242+0049 with different physical properties may arise at different type of absorbers at very different radial distances, as sometimes suggested for BAL absorbers. The former could be the outflow winds at large distance that are interacting with ISM and CGM of host galaxies.

(v) BAL and intrinsic NAL absorbers could be closely related each other because both class of absorbers locate at wide range of radial distance along same LOS. Thus, our results suggest that absorption width does not simply de-

depends on the inclination angle, but also depends on internal structure of outflow winds.

As a future work, we will increase our sample size at least by a factor of three to match the sample size for non-BAL quasars (37 in Misawa et al. 2007) to investigate how the detection rate of intrinsic NALs depends on the co-existence of BAL features along same LOS. We also need to spectroscopically identify the point source at ~ 5 arcsec north-west of J1215-0034 to narrow down possible origins of the class B NAL absorber with a quite large radial distance of ≥ 130 kpc (i.e., a large distance outflow or an unusual intervening absorber with a partial coverage in a foreground galaxy).

ACKNOWLEDGEMENTS

The research was supported by the Japan Society for the Promotion of Science through Grants-in-Aid for Scientific Research 18K03698.

Based on observations made with ESO Telescopes at the La Silla Paranal Observatory under programs, 081.A-0479(A), 075.B-01908A9, 083.A-0042(A), 092.B-0574(A), 079.B-0479(A), 273.A-5020(A), 080.A-0482(A), 185.A-0745(D), 081.A-0334(A), 091.A-0018(A), 081.B-0285(A).

DATA AVAILABILITY

The datasets underlying this article were derived from sources in the public domain as given in the respective footnotes.

REFERENCES

Aoki K., Oyabu, S., Dunn J. P., Arav N., Edmonds D., Korista K., T., Matsuhara H., Toba Y., 2011, PASJ, 63, 617
 Arav N., 1996, ApJ, 465, 617
 Arav N., Borguet B., Chamberlain C., Edmonds D., Danforth C., 2013, MNRAS, 465, 457
 Arav N., Liu G., Xu X., Stidham J., Benn C., Chamberlain C., 2018, ApJ, 857, 60
 Balashev S. A., Ledoux C., Noterdaeme P., Srianand R., Petitjean P., Gupta N., 2020, arXiv:2007.07707
 Bañados E., et al., 2015, ApJ, 804, 118
 Barlow T. A., Hamann F., Sargent W. L. W., 1997, in Astronomical Society of the Pacific Conference Series, Vol. 128, Mass Ejection from Active Galactic Nuclei, Arav N., Shosman I., Weymann R. J., eds., p. 13
 Barlow T. A., Sargent W. L. W., 1997, AJ, 113, 136
 Becker R. H., Gregg M. D., Hook I. M., McMahon R. G., White R. L., Helfand D. J., 1997, ApJ, 479, L93
 Boroson T. A., Meyers K. A., 1992, ApJ, 397, 442
 Borguet B. C. J., Edmonds D., Arav N., Dunn, J., Kriss G. A., 2012, ApJ, 751, 107
 Borguet B. C. J., Arav N., Edmonds D., Chamberlain C., Benn C., 2013, ApJ, 762, 49
 Bruni G., et al., 2019, A&A, 630, A111
 Capellupo D. M., Hamann F., Shields J. C., Rodríguez Hidalgo P., Barlow T. A., 2011, MNRAS, 413, 908
 Chamberlain C., Arav N., Benn C., 2015, MNRAS, 450, 1085

Chartas G., et al., 2009, New Astronomy Reviews, 53, 128
 Chelouche D., Netzer H., 2005, ApJ, 625, 95
 Chen C., Hamann F., Simon L., Barlow T., 2018, MNRAS, 481, 3865
 Churchill C. W., Vogt S. S., 2001, AJ, 122, 679
 Di Matteo T., Springel V., Hernquist L., 2005, Nature, 433, 604
 Dunn J. P., et al., 2010, ApJ, 709, 611
 Elvis M., 2000, ApJ, 545, 63
 Everett J. E., 2005, ApJ, 631, 689
 Farrah D., Lacy M., Priddey R., Borys C., Afonso J., 2007, ApJL, 662, L59
 Faucher-Giguère C.-A., Quataert E., Murray N., 2012, MNRAS, 420, 1347
 Foltz C. B., Weymann R. J., Peterson B. M., Sun L., Malkan M. A., Chaffee F. H., 1986, ApJ, 307, 504
 Ganguly R., Eracleous M., Charlton J. C., Churchill C. W., 1999, AJ, 117, 2594
 Ganguly R., Bond N. A., Charlton J. C., Eracleous M., Brandt W. N., Churchill C. W., 2001, ApJ, 549, 133
 Ganguly R., Brotherton M. S., Cales S., Scoggins B., Shang Z., Vestergaard M., 2007, ApJ, 665, 990
 Ganguly R., et al., MNRAS, 2013, 435, 1233
 Gehrels N., 1986, ApJ, 303, 336
 Gibson R. R., et al., 2009, ApJ, 692, 758
 Giustini M., Proga D., 2019, A&A, 630, 94
 Goldsmith P. F., Langer W. D., Pineda J. L., Velusamy T., 2012, ApJS, 203, 13
 Hacker T. L., Brunner R. J., Lundgren B. F., York D. G., 2013, MNRAS, 434, 163
 Hall P. B., Sadavoy S. I., Hutsemekers D., Everett J. E., Rafiee A., 2007, ApJ, 665, 174
 Hamann F. W., Barlow T. A., Chaffee F. C., Foltz C. B., Weymann R. J., 2001, ApJ, 550, 141
 Hamann F., Chartas G., Reeves J., Nardini E., 2018, MNRAS, 476, 943
 Hamann F., Simon L., Rodríguez Hidalgo P., Capellupo D., 2012, AGN Winds in Charleston, 460, 47
 Hamann F., 1997, ApJS, 109, 279
 Hamann F., Barlow T. A., Junkkarinen V., Burbidge E. M., 1997, ApJ, 478, 80
 Hayashi T. J., Doi A., Nagai H., 2013, ApJ, 772, 4
 Hazard C., McMahon R. G., Webb J.K., Morton D. C., 1987, ApJ, 323, 263
 Hemler Z. S., et al., 2019, ApJ, 872, 21
 Hutsemekers D., Hall P. B., Brinkmann J., 2004, A&A, 415, 77
 Ivezić Ž., et al., 2002 AJ, 124, 2364
 Jiang L., Fan X., Ivezić Ž., Richards G. T., Schneider D. P., Strauss M. A., Kelly B. C., 2007 ApJ, 656, 680
 Jones T. M., Misawa T., Charlton J. C., Mshar A. C., Ferland G. J., 2010, ApJ, 715, 1497
 Kellermann K. I., Sramek R., Schmidt M., Shaffer D. B., Green R., 1989, AJ, 98, 1195
 Kobayashi H., Ohsuga K., Takahashi H. R., Kawashima T., Asahina Y., Takeuchi S., Mineshige S., 2018, PASJ, 70, 22
 Lira P., et al., 2018, ApJ, 865, 56
 Lu W.-J., Lin Y.-R., 2018a, MNRAS, 474, 3397
 Lu W.-J., Lin Y.-R., 2018b, ApJ, 863, 186
 Lu W.-J., Lin Y.-R., 2019, ApJ, 881, 105L
 Lusso E., Worseck G., Hennawi J. F., Prochaska J. K., Vignali C., Stern J., O’Meara J. M., 2015, MNRAS, 449, 4204
 Martocchia S., et al. 2017, A&A, 608, A51
 Mathews W. G., Ferland G. J., 1987, ApJ, 323, 456
 McGraw S. M., et al., 2017, MNRAS, 469, 3163
 Misawa T., Eracleous M., Chartas G., Charlton J. C., 2008, ApJ, 677, 863
 Misawa T., Charlton J. C., Eracleous M., Ganguly R., Tytler D., Kirkman D., Suzuki N., Lubin D., 2007, ApJS, 171, 1
 Misawa T., Charlton J. C., Eracleous M., 2014, ApJS 792, 77

- Moe M., Arav N., Bautista M. A., Korista K. T., 2009, *ApJ*706, 525
- Moravec E. A., Hamann F., Capellupo D. M., McGraw S. M., Shields J. C., Rodriguez Hidalgo P., 2017, *MNRAS*, 468, 4539
- Morris S. L., Weymann R.J., Foltz C. B., Turnshek D. A., Shectman S., Price C., Boroson T. A., 1986, *ApJ*, 310, 40
- Murray N., Chiang J., Grossman S. A., Voit G. M., 1995, *ApJ*, 451, 498
- Muzahid S., Srianand R., Charlton J., Eracleous M., 2016, *MNRAS*, 457, 2665
- Nestor D., Hamann F., Rodriguez Hidalgo P., 2008, *MNRAS*, 386, 2055
- Ohsuga K., Mori M., Nakamoto T., Mineshige S., 2005, *ApJ*, 628, 368
- Proga D., Stone J. M., Kallman T. R., 2000, *ApJ*, 543, 686
- Proga D., Kallman, T. R., 2004, *ApJ*, 616, 688
- Proga D., Rodriguez Hidalgo P., Hamann F., 2012, in *Astronomical Society of the Pacific Conference Series*, Vol. 460, AGN winds in Charleston, ed. G. Chartas, F. Hamann, K. M. Leighly, 171
- Reichard T. A., et al., 2003, *AJ*, 126, 2594
- Rodriguez Hidalgo P., 2009, Ph.D. thesis, University of Florida, United States - Florida
- Rodriguez Hidalgo P., Hamann F., Hall P., 2011, *MNRAS*, 411,247
- Sargent W. L. W., Boksenberg A., Young P., 1982, *ApJ*, 252, 54
- Savage B. D., Sembach K. R., 1991, *ApJ*, 379, 245
- Simon L. E., Hamann F., Pettini M., 2012, *AGN Winds in Charleston*, 460, 52
- Takeuchi S., Ohsuga K., Mineshige S., 2013, *PASJ*, 65, 88
- Tolea A., Krolik J. H., Tsvetanov Z., 2002, *ApJ*, 578, L31
- Tripp T. M., Lu L., Savage B. D., 1996, *ApJS*, 102, 239
- Trump J. R., et al., 2006, *ApJS*, 165, 1
- Tumlinson J., Peebles M. S., Werk J. K., 2017, *Annual Review of Astronomy and Astrophysics*, 55, 389
- Urry C. M., Padovani P., 1995, *PASP*, 107, 803
- Voit G. M., Weymann R. J., Korista K. T., 1993, *ApJ*, 413, 95
- Wall J. V., Shimmins A. J., Merkelijn K., 1971, *Aust. J. Phys., Astrophys., Suppl*, 19, 1
- Weymann R. J., Morris S. L., Foltz C. B., Hewett P. C., 1991, *ApJ*, 373, 23
- Weymann R. J., Williams R. E., Peterson B. M., Turnshek D. A., 1979, *ApJ*, 234, 33
- Wiid V., et al., 2008, *MNRAS*, 613, 129
- Wise J. H., Eracleous M., Charlton J. C., Ganguly R., 2004, *ApJ*, 613, 129
- Wright A. E., Morton D. C., Peterson B. A., Jauncey D.L., 1979, *MNRAS*, 189, 611
- Wu J., Charlton J. C., Misawa T., Eracleous M., Gangly R., 2010, *ApJ*, 722, 997
- Xu X., Arav N., Miller T., Benn C., 2018, *ApJ*, 858, 39

This paper has been typeset from a $\text{\TeX}/\text{\LaTeX}$ file prepared by the author.